



# Evidence for a vanishing ${}^6\text{Li}/{}^7\text{Li}$ isotopic signature in the metal-poor halo star HD 84937

K. Lind<sup>1</sup>, M. Asplund<sup>2</sup>, R. Collet<sup>1,3,4</sup>, and J. Meléndez<sup>5</sup>

- <sup>1</sup> Max Planck Institute for Astrophysics, Karl-Schwarzschild-Str. 1, 85741, Garching, Germany e-mail: klind@mpa-garching.mpg.de  
<sup>2</sup> Research School of Astronomy & Astrophysics, Mount Stromlo Observatory, Cotter Road, Weston Creek, ACT 2611  
<sup>3</sup> Centre for Star and Planet Formation, Natural History Museum of Denmark University of Copenhagen, Øster Voldgade 5-7, DK-1350 Copenhagen, Denmark  
<sup>4</sup> Astronomical Observatory/Niels Bohr Institute, Juliane Maries Vej 30, DK2100 Copenhagen, Denmark  
<sup>5</sup> Departamento de Astronomia do IAG/USP, Universidade de São Paulo, Rua do Matão 1226, Cidade Universitária, 05508-900 São Paulo, SP, Brasil

**Abstract.** The claimed detections of  ${}^6\text{Li}$  in the atmospheres of some metal-poor halo stars have lead to speculative additions to the standard model of Big Bang nucleosynthesis and the early Universe, as the inferred abundances cannot be explained by Galactic cosmic ray production. A prominent example of a so far un-disputed  ${}^6\text{Li}$ -detection is that of the metal-poor turn-off star HD 84937, for which at least three different groups obtain very similar results. We revisit the lithium isotopic analysis for this star and two other halo stars, G 64-12 and HD 140283, using spectra of superior quality and applying for the first time a combined 3D, NLTE synthesis to both the Li line and to Ca lines that are used to constrain the external line broadening. We demonstrate how differential NLTE effects between the Li and Ca line profiles can lead to spurious  ${}^6\text{Li}$ -detections in LTE, compatible with previously reported values of  ${}^6\text{Li}/{}^7\text{Li} \approx 5\%$ . With our new analysis technique, none of the three analysed stars have a significant detection of  ${}^6\text{Li}$  in NLTE. We discuss which further progress is needed to firmly establish these results.

**Key words.** Line: profiles – Stars: Population II – Stars: individual: (HD 84937, HD 140283, G 64-12 – Hydrodynamics – Radiative transfer

## 1. Introduction

It is widely accepted that the  ${}^7\text{Li}$ -abundance plateau of very metal-poor un-evolved stars is the progeny of primordial nucleosynthesis. That the so called Spite plateau-value falls short of the expectations by a factor of 2 – 5 (e.g. Meléndez et al. 2010; Sbordone et al.

2010) may be subscribed at least partly to internal diffusion processes (e.g. Richard et al. 2005; Korn et al. 2007), altering the surface abundances of low mass stars over time. However, if these are truly at work, it would further aggravate the second cosmological Li problem, which concerns the abundances of the lighter of the two stable Li isotopes. The

positive  ${}^6\text{Li}/{}^7\text{Li}$ -ratios of typically 5% that have been reported for some very metal-poor halo stars (Smith et al. 1993, 1998; Asplund et al. 2006; Steffen et al. 2010; Asplund & Lind 2010) are already very difficult to explain in the framework of a standard Big Bang and subsequent cosmic ray spallative production. That  ${}^6\text{Li}$  is even more easily destroyed than  ${}^7\text{Li}$  worsens the problem. The primordial contribution of  ${}^6\text{Li}$  is insignificant in this context unless a non-standard ingredient is invoked, e.g. the decay of heavy super-symmetric particles (e.g. Jedamzik & Pospelov 2009). Other pre-Galactic production sources, such as particle acceleration by massive stars, black hole jets, or structure formation-induced shocks are not nearly energetic enough to produce the necessary amounts of the lighter isotope on a cosmic scale, although they may contribute locally (Prantzos 2012, and references therein). It is of great importance for our understanding of the early Universe that the  ${}^6\text{Li}$  levels of the oldest stars are precisely and quantitatively constrained.

Given that the presence of the lighter isotope manifests itself as a very mild asymmetry in an intrinsically asymmetric, fine-structure doublet, the measurement is extraordinarily challenging both from the observational and modelling point of view. Only with the highest quality spectra that modern telescopes can provide can the error bars on the isotopic ratio reach the necessary  $\sim 1 - 2\%$  level. The modelling must realistically capture all broadening agents that enter the spectral line formation as well as the departures from LTE. Some authors, e.g. Cayrel et al. (2007) and Asplund & Meléndez (2008), have therefore stressed the need for verifications of all  ${}^6\text{Li}$ -detections by NLTE modelling in 3D hydrodynamical model atmospheres. In these proceedings we present for the first time a combined 3D, NLTE approach for the modelling of lithium as well as other lines used as diagnostics of the external line broadening.

For these proceedings we selected three well-known halo stars that sample the metallicity range  $-3.2 < [\text{Fe}/\text{H}] < -2.1$ ; HD 84937 ( $[\text{Fe}/\text{H}] \sim -2.1$ ), HD 140283 ( $[\text{Fe}/\text{H}] \sim -2.4$ ) and G 64-12 ( $[\text{Fe}/\text{H}] \sim -3.2$ ). These stars have

been previously studied for  ${}^6\text{Li}$  (e.g. Smith et al. 1993, 1998; Aoki et al. 2004; Asplund & Meléndez 2008; Cayrel et al. 1999), hence we can compare our results to those previous works (see Sec. 5).

## 2. Analysis

### 2.1. Observed data

The observed data were collected with HIRES at the 10 m Keck I telescope, in different observing runs during 2005 and 2006. The observed Keck/HIRES spectra were acquired at a spectral resolving power of  $\lambda/\Delta\lambda = 90,000 - 100,000$  and signal-to-noise of  $S/N = 800 - 1100$  per pixel around the Li i 6708Å line. The data were reduced by hand with IRAF and we also tried the MAKEE program. Different tests were performed and independently of the adopted approach essentially similar results were obtained, well constraining the important asymmetry in the red part of the Li profile.

### 2.2. 3D modelling

To infer the  ${}^6\text{Li}$  and  ${}^7\text{Li}$  isotopic abundances requires the ability to model the intrinsic line shapes. Of particular importance is the realistic capture of line broadening due to convective motions and rotation. Here, we have chosen to model the former using 3D hydrodynamic convection simulations and incorporate any remaining external broadening in addition to the instrumental profile in the unknown projected rotational velocity  $v_{\text{rot}} \sin i$ . In addition to the Li line itself, we use a set of neutral and singly ionised lines of several species to put constraints on this parameter. By accounting for the full 3D velocity cube in the spectrum synthesis, we model the intrinsic asymmetry of the lines that arise naturally due to convection and are not dependent on the free parameters that are inherent in traditional 1D modelling (micro- and macroturbulence).

The STAGGER code (Collet et al. 2011) was utilized to compute the models for the three investigated stars, with model parameters as summarised in Table 1. LTE synthesis was performed on 20 individual snapshots (240<sup>3</sup> grid

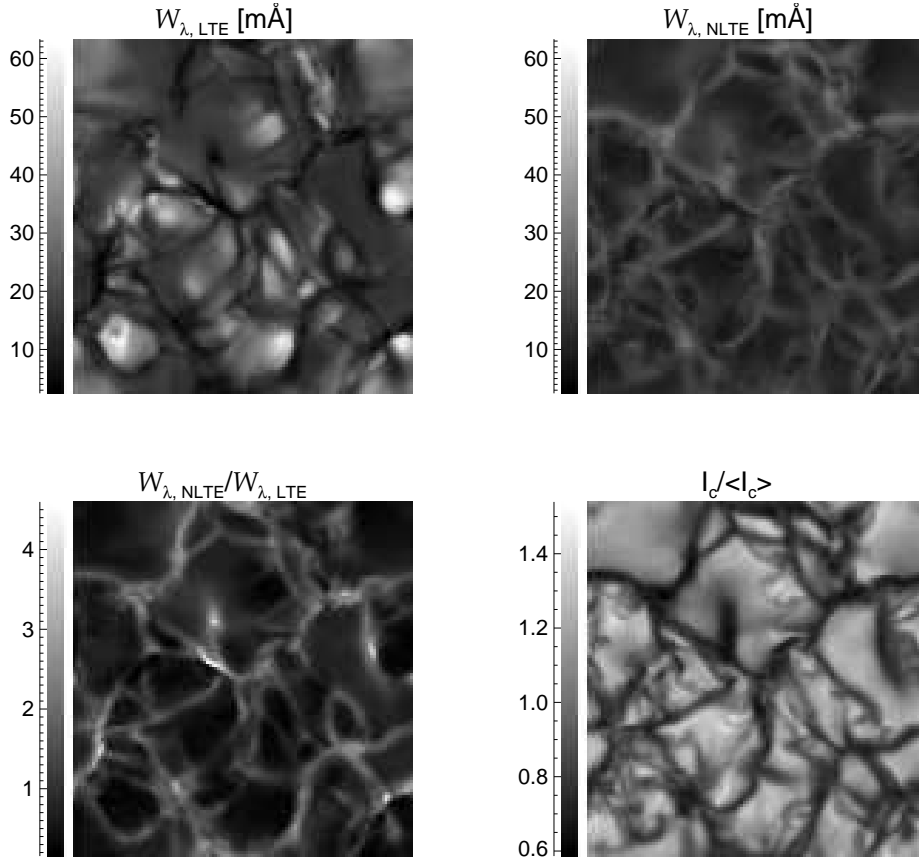


Fig. 1: The top panels show spatially resolved LTE and NLTE equivalent widths of the Li I 6707Å line in one snapshot of the 3D model of HD 84937, for a Li abundance of  $A(\text{Li}) = 2.0$ . The mean values and one sigma dispersions are in the two cases,  $\langle W_{\lambda, \text{LTE}} \rangle = 19.0 \pm 8.5 \text{ mÅ}$  and  $\langle W_{\lambda, \text{NLTE}} \rangle = 14.6 \pm 4.0 \text{ mÅ}$ . The bottom left panel indicates the ratio between two and the bottom right panel shows the simulated relative continuum intensity.

points), at  $6\mu \times 4\phi$  different angles using the code SCATE (Hayek et al. 2011). The spatial and temporal mean surface flux profile was then formed and compared to observations after convolution with the instrumental profile and the rotational velocity profile.

### 2.3. NLTE modelling

The formation of the 6707Å Li I resonance line is not well described by the LTE assump-

tion, especially not in metal-poor, 3D model atmospheres (e.g. Carlsson et al. 1994; Asplund et al. 2003; Lind et al. 2009). Considering that not only the line strength, but also the shape of the line profile is subject to NLTE effects, a combined 3D and NLTE approach is necessary. We have used the 3D statistical equilibrium code MULTI3D (Botnen 1997; Leenaarts et al. 2010), which is based on the widely used 1D NLTE code MULTI (Carlsson 1986; Carlsson et al. 1994). MULTI3D is a domain decomposed and MPI-parallellised code for sta-

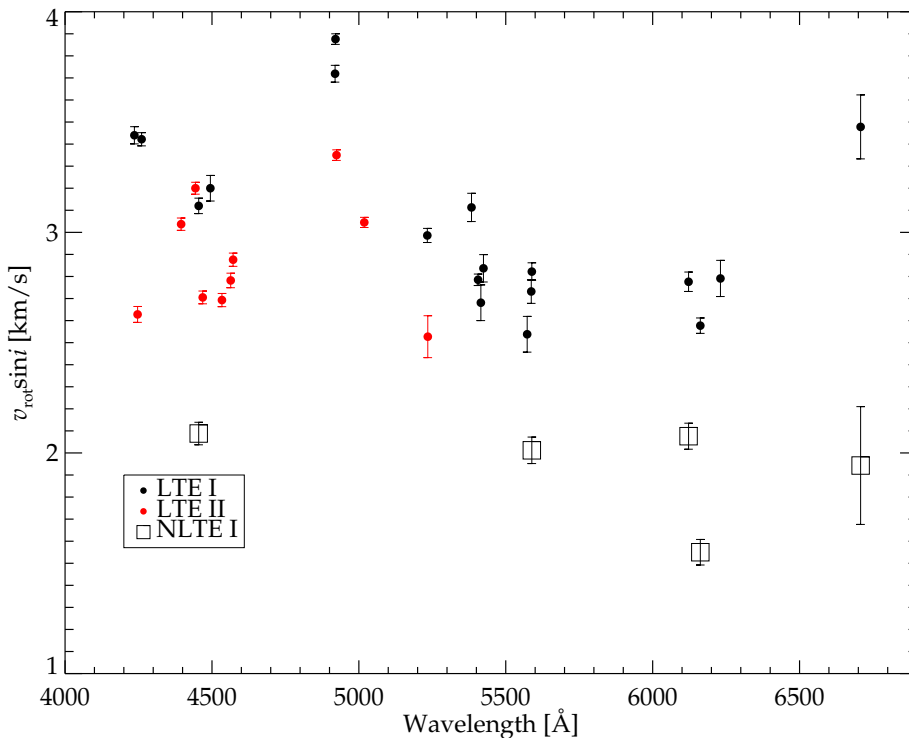


Fig. 2: The panels show the projected rotational velocities as estimated from lines of different species and ionisation stages for HD 84937. For Li,  $^6\text{Li}/^7\text{Li} = 0$  is assumed here. The black and grey (red in the online version) bullets represent lines of neutral (Li I, Ca I, Fe I) and singly ionized ions (Ti II, Sc II, Fe II), respectively.

Table 1: Adopted model stellar parameters and derived  $^7\text{Li}$  and Ca abundances. The line-by-line abundance dispersion is indicated for Ca.

Star	$T_{\text{eff}}$	$\log g$	[Fe/H]	LTE			NLTE		
				$A(^7\text{Li})$	$A(\text{Ca})$	$\sigma$	$A(^7\text{Li})$	$A(\text{Ca})$	$\sigma$
G 64-12	6428	4.2	-3.0	2.12	3.49	0.06	2.23	3.64	0.04
HD 140283	5750	3.7	-2.5	1.84	3.91	0.10	2.13	4.21	0.05
HD 84937	6238	4.0	-2.0	1.95	4.37	0.10	2.15	4.63	0.04

tistical equilibrium and radiative transfer calculations, which sets a self-consistent radiation field and atomic level populations.

To compute the NLTE level populations, the 21-level Li model atom developed by Lind et al. (2009) was used with minor modifica-

tions. The atom contains 100 radiative bound-bound transitions and photo-ionization to the Li II ground state. All levels are coupled by collisions with electrons and hydrogen atoms, including the quantum mechanical calculations by (Barklem et al. 2003). We let MULTI3D

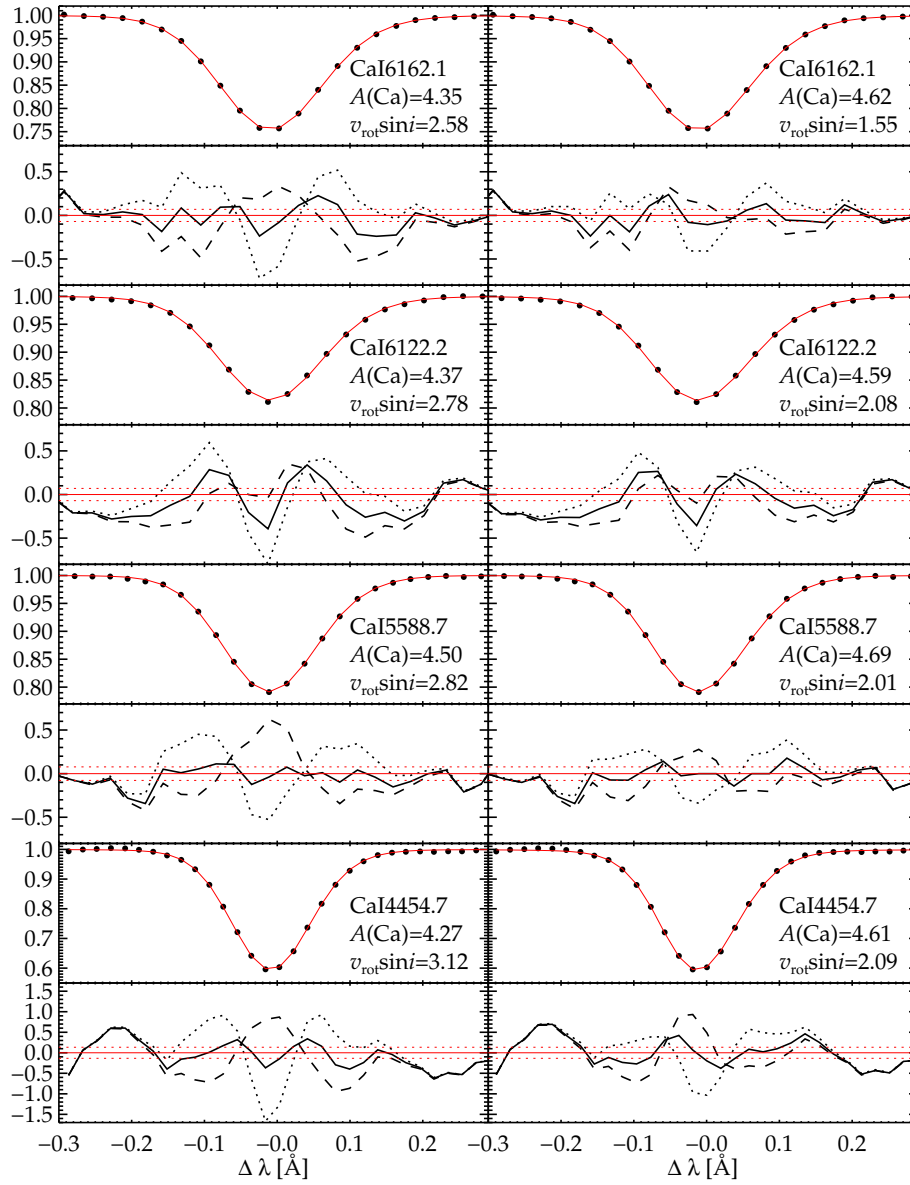


Fig. 3: Observed spectra (filled bullets) and synthetic spectra (solid lines) of the Ca I lines used for determination of  $v_{\text{rot}} \sin i$  for HD 84937. LTE synthesis is displayed in the left hand panels and NLTE synthesis in the right hand panels. The flux residuals in percent are displayed below each line profile. The solid line indicates the best fit and the dotted and dashed lines represent rotational velocities that are higher and lower by  $0.5 \text{ km s}^{-1}$ , respectively. The Ca abundance is a free parameter in all fits. The horizontal dotted lines mark the estimated noise level.

Table 2: Lithium isotopic ratios and projected rotational velocities determined in LTE and NLTE. In cases (a), the rotational velocity is determined from the Li line itself, while in cases (b), it is determined from other spectral lines. For details, see text.

Star	LTE (a)		NLTE (a)	
	$v \sin i$	$^6\text{Li}/^7\text{Li}$	$v \sin i$	$^6\text{Li}/^7\text{Li}$
G 64-12	$3.20 \pm 0.23$	$0.035 \pm 0.019$	$1.14 \pm 0.64$	$0.021 \pm 0.012$
HD 140283	$3.20 \pm 0.08$	$0.020 \pm 0.005$	$1.50 \pm 0.12$	$-0.004 \pm 0.002$
HD 84937	$2.97 \pm 0.17$	$0.030 \pm 0.012$	$1.60 \pm 0.32$	$0.007 \pm 0.005$
Star	LTE (b)		NLTE (b)	
	$v \sin i$	$^6\text{Li}/^7\text{Li}$	$v \sin i$	$^6\text{Li}/^7\text{Li}$
G 64-12	$2.79 \pm 0.21$	$0.052 \pm 0.011$	...	...
HD 140283	$1.95 \pm 0.13$	$0.054 \pm 0.004$	...	...
HD 84937	$2.71 \pm 0.05$	$0.042 \pm 0.008$	$1.88 \pm 0.17$	$0.001 \pm 0.005$
Star	Calibrating lines LTE		Calibrating lines NLTE	
G 64-12	MgI 5172		...	
	FeI 4920, 5227		...	
HD 140283	CaI 5588, 6122, 6162		...	
	FeI 5572, 5586, 6230		...	
HD 84937	CaI 5588, 6122, 6162		CaI 5588, 6122, 6162	
	FeI 5572, 5586, 6230			

solve the statistical equilibrium equations in each vertical column separately with a standard 1D radiative transfer scheme, a so called 1.5D radiative transfer calculation. Once the NLTE level populations had converged, the cube was tilted at different angles to compute the full 3D emergent flux profiles. Due to the computationally demanding nature of 3D NLTE radiative transfer, calculations with MULTI3D were only performed on four snapshots per star, after which the average NLTE/LTE line profile ratio was multiplied with the better sampled LTE line profile computed with SCATE at constant abundance.

In addition to Li, a handful of neutral Ca lines were also treated with the same approach in NLTE. A newly developed 45-level Ca model atom was used (39 levels of Ca I, 5 levels of Ca II, and the Ca III ground state), coupled by  $\sim 250$  radiative transitions. Energy levels were assembled from the NIST database (Ralchenko et al. 2008), oscillator strengths primarily from the Kurucz database, and photo-ionisation cross-sections from the TOP base (H. E. Saraph & P. J. Storey, to be

published)<sup>1</sup>. Electronic collisions were taken from quantum mechanical calculations whenever possible (Samson & Berrington 2001; Meléndez et al. 2007), complemented with the general recipes of Allen (2000). Hydrogen collisions were included according to the Drawin recipe (Drawin 1968), following the implementation of Lambert (1993), with a scaling factor of 0.1 (Mashonkina et al. 2007).

The NLTE effects on the total Li line strengths are dramatic, as displayed in Fig. 1 for the model of HD 84937. While the line is weakened in NLTE due to efficient ionisation in the bright granules, the intergranular lanes suffer from the opposite effect, strengthening the line significantly compared to LTE. The combined effect on the average flux profile is nevertheless dominated by the over-ionisation effect, and the line strength is significantly di-

<sup>1</sup> Links to online data bases:

<http://physics.nist.gov/asd>,  
<http://www.pmp.uni-hannover.de/cgi-bin/ssi/test/kurucz/sekur.html>,  
<http://cdsweb.u-strasbg.fr/topbase/topbase.html>

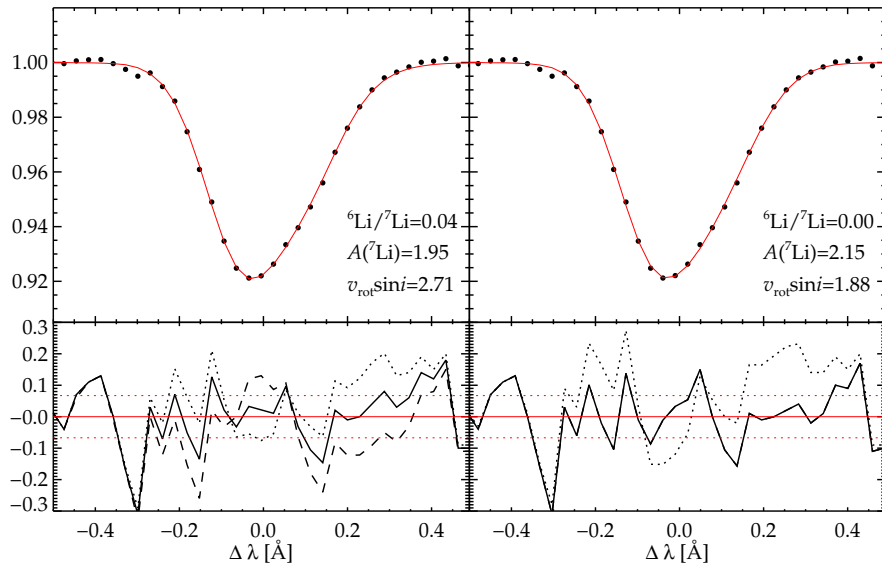


Fig. 4: Observed (filled bullets) and synthetic spectra (solid lines) of the LiI resonance doublet in HD 84937. LTE synthesis is displayed in the left hand panels and NLTE synthesis in the right hand panels. The flux residuals in percent are displayed below each line profile. For the LTE case, the residuals are shown for three different Li isotopic ratios; 0.00 (dashed line), 0.04 (solid line), and 0.08 (dotted line). For the NLTE case, two values are shown; 0.00 (solid line) and 0.04 (dotted line). The external line broadening has been determined from other spectral lines, modelled consistently in LTE and NLTE (see Table 2). The horizontal dotted lines mark the estimated noise level.

minished in NLTE (see also Asplund et al. 2003; Cayrel et al. 2007). However, the NLTE effects also significantly alters the line shape compared to LTE, which impacts on the projected rotational velocities determined from observed spectra.

### 3. Results

#### 3.1. Projected rotational velocity

To constrain the external line broadening, here incorporated in  $v_{\text{rot}} \sin i$ , we have modelled a number of spectral lines of different species and ionisation stages. The line selection criteria are balanced between the need to minimize systematic biases and maintaining necessary statistics. First, the lines should be situated close to the lithium line, thereby having similar continuous opacities and similar response to wavelength-dependent phenomena, like Doppler broadening and spectral resolu-

tion variations. Second, the lines should not be too strong ( $< 80 \text{ m}\text{\AA}$ ), i.e. not too strongly influenced by pressure broadening, and not too weak ( $> 10 \text{ m}\text{\AA}$ ) to make the measurement uncertain. Ideally, the line strength should be as similar as possible to the Li 6707Å line.

Fig. 2 shows the rotational determined from lines in HD 84937. Evidently, LTE analysis overestimates the external broadening compared to NLTE for both Li and Ca lines, and more so for the former. In general, neutral lines give higher rotational broadening than singly ionised lines at a given wavelength, probably indicating that the selected FeI lines suffer from similar NLTE broadening effects as Li I and Ca I lines. Hypothetically, it is not unreasonable to assume that the NLTE effects would cancel out if one uses LTE consistently for the calibrating lines and the Li I line. However, it appears from the figure that the Li I line is actually more severely affected than the Ca I lines.

This is of critical importance for the determination of the isotopic ratio, as discussed in the next section.

It is also evident from Fig. 2 that bluer lines tend to give larger velocities than redder lines, which partly may be subscribed to a small increasing trend in  $v_{\text{rot}} \sin i$  with increasing line strength. This could imply minor shortcomings in the modelling of intrinsic line broadening or of the instrumental profile and we regard the lines closest to the Li I line in wavelength and equivalent width as the most unbiased indicators. We note that the 3D models reproduce remarkably well the line shapes and asymmetries in the Sun, Procyon, and the metal-poor giant HD 122563 (e.g. Asplund et al. 2000; Allende Prieto et al. 2003; Ramírez et al. 2010).

Fig. 3 shows the line profile synthesis of four Ca I lines in HD 84937, in LTE and NLTE. These fits to the observed lines are obtained by optimising the continuum placement, the radial velocity, the rotational velocity, and the Ca abundance through  $\chi^2$ -minimization, after convolving the synthetic spectra with the measured instrumental broadening. As can be seen in the flux residuals in Fig. 3 and in the error bars of Fig. 2, the rotational broadening is somewhat better constrained in LTE than NLTE. This reflects the difference in line profile shape, with the NLTE profiles being broader and shallower at a given line strength and  $v_{\text{rot}} \sin i$ .

### 3.2. Lithium isotopic abundances

The  $\chi^2$ -surface for the Li line reveals a degeneracy between the  ${}^7\text{Li}$  abundance,  $v_{\text{rot}} \sin i$ , and  ${}^6\text{Li}/{}^7\text{Li}$ . The higher the rotational broadening adopted, the higher the best fitting  ${}^7\text{Li}$  abundance, at the expense of a lower isotopic ratio. With our high-quality observations, a well-defined minimum can however be found using only the information in the line itself. In a first approach, we thus kept all three parameters free, in addition to the radial velocity and the continuum placement. We computed  $\chi^2 = \sum(\text{obs} - \text{syn})^2 \times (\text{S/N})^2$  for 20 different values of  ${}^6\text{Li}/{}^7\text{Li}$  and re-optimised the remaining parameters each time. The best fitting isotopic ratio was then found at the minimum

of a quadratic fit to the  $\chi^2$ -curve, allowing for extrapolation to negative values, and the  $1\sigma$ -error was found where  $\chi^2 - \chi_{\text{min}}^2 = 1$ . In a second approach, we used other lines to constrain the external broadening and thus removed one free parameter in the fit of the Li line. The calibration lines were modelled consistently with the Li line, either in LTE or NLTE. All results are presented in Table 2 and the synthesis of Li 6707Å line in HD 84937 illustrated in Fig. 4.

Evidently,  ${}^6\text{Li}$  detections that are significant on a  $2\sigma$ -level are only encountered in LTE, suggesting that they are artifacts of this simplifying assumption. In NLTE, no significant contribution from the lighter isotope is needed to reproduce the line profiles. Using only the information in the Li line itself, all stars are found to have isotopic ratios of 2–3% assuming LTE, while they are consistent with zero in NLTE. Note that the  $\chi^2$ -curve is more well defined in NLTE, resulting in a smaller error bar on the isotopic ratio than in LTE.

For all three stars the ratios are magnified to 4–5% in LTE if other lines are used for calibration of line broadening (LTE (b)), since the calibrating Mg I, Ca I and Fe I lines indicate lower values of the projected rotational velocity. For HD 84937, we were able to constrain the rotational broadening also from NLTE analysis of the Ca I lines, in good agreement with the results obtained for the Li I line in NLTE. The calibrating lines thus support a vanishing contribution of  ${}^6\text{Li}$  in this star. For the other two stars, a more extensive NLTE analysis is needed to verify the rotational velocity obtained from the Li line.

## 4. Discussion

The three stars analysed here have had their lithium isotopic ratios investigated previously, with varying conclusions. The most recent measurements for all three stars were reported by Asplund & Meléndez (2008), who found  $5.9 \pm 2.1\%$  for G 64-12,  $1.7 \pm 1.0\%$  for HD 140283, and  $5.1 \pm 1.5\%$  for HD 84937 based on a 1D/3D LTE analysis. In addition, Aoki et al. (2004) report  $< 1.8\%$  in 1D LTE for HD 140283 and Steffen et al. (2010) give a 3D, NLTE result of 5.2% for HD 84937. The

latter star has also been analysed by Smith et al. (1993), Smith et al. (1998), and Hobbs & Thorburn (1997), all concluding a significant  ${}^6\text{Li}/{}^7\text{Li}$ -detection on the  $\sim 5\%$ -level.

Considering the difficulties involved in the measurement, there are numerous plausible explanations for differences with respect to earlier work, including the observed data used, model atmospheres in 1D or 3D, LTE or NLTE synthesis, and the method used to constrain broadening (e.g. assumed shape of convolving function, selection criteria and number of calibration lines). However, it is notable that irrespectively of the developments in analysis methods, HD 84937 has up until now had a remarkably un-disputed  ${}^6\text{Li}$ -detection ever since the first measurement almost two decades ago by Smith et al. (1993). In this work, we have illustrated how detections found through LTE analysis can be artifacts of this commonly adopted assumption. However, before we can regard the non-detections for our stars with a high level of confidence there are still a number of outstanding issues that must be resolved, in particular differences that still exist with respect to Asplund & Meléndez (2008) and Steffen et al. (2010) when the same methodology is adopted. For example, Steffen et al. (2010) value for HD 84937 was obtained by 3D, NLTE analysis and should thus be compared with our non-detection (NLTE (a),  $0.7 \pm 0.5\%$ ). Potentially, our significantly improved spectrum quality, with almost twice as high S/N-ratio, can be held responsible for the different conclusions.

Constraining five free parameters from a single spectral line is venturesome even with the best possible observational quality, and we demonstrate the results of this method here mainly for comparison purposes. Only by making full use of all the information imprinted also on other spectral lines can the quality of the results be correctly assessed. Both the external line broadening and the mean radial velocity can and should be verified with consistent modelling of other spectral lines, thereby also understanding potential systematic biases between lines with different characteristics. More work is clearly needed to firmly con-

strain the  ${}^6\text{Li}$ -abundances of these and other metal-poor stars.

## References

- Allen, C. W. 2000, *Allen's Astrophysical Quantities*, 4th edn. (Springer, Berlin)
- Allende Prieto, C., Hubeny, I., & Lambert, D. L. 2003, *ApJ*, 591, 1192
- Aoki, W., Inoue, S., Kawanomoto, S., et al. 2004, *A&A*, 428, 579
- Asplund, M., Carlsson, M., & Botnen, A. V. 2003, *A&A*, 399, L31
- Asplund, M., Lambert, D. L., Nissen, P. E., Primas, F., & Smith, V. V. 2006, *ApJ*, 644, 229
- Asplund, M. & Lind, K. 2010, in *IAU Symposium*, Vol. 268, *IAU Symposium*, ed. C. Charbonnel, M. Tosi, F. Primas, & C. Chiappini, 191–200
- Asplund, M. & Meléndez, J. 2008, in *American Institute of Physics Conference Series*, Vol. 990, *First Stars III*, ed. B. W. O'Shea & A. Heger, 342–346
- Asplund, M., Nordlund, Å., Trampedach, R., Allende Prieto, C., & Stein, R. F. 2000, *A&A*, 359, 729
- Barklem, P. S., Belyaev, A. K., & Asplund, M. 2003, *A&A*, 409, L1
- Botnen, A. 1997, Master's thesis, Master's thesis, *Inst. Theor. Astrophys. Oslo* (1997)
- Carlsson, M. 1986, *Uppsala Astronomical Observatory Reports*, 33
- Carlsson, M., Rutten, R. J., Bruls, J. H. M. J., & Shchukina, N. G. 1994, *A&A*, 288, 860
- Cayrel, R., Spite, M., Spite, F., et al. 1999, *A&A*, 343, 923
- Cayrel, R., Steffen, M., Chand, H., et al. 2007, *A&A*, 473, L37
- Collet, R., Magic, Z., & Asplund, M. 2011, *ArXiv e-prints*
- Drawin, H.-W. 1968, *Zeitschrift fur Physik*, 211, 404
- Hayek, W., Asplund, M., Collet, R., & Nordlund, Å. 2011, *A&A*, 529, A158
- Hobbs, L. M. & Thorburn, J. A. 1997, *ApJ*, 491, 772
- Jedamzik, K. & Pospelov, M. 2009, *New Journal of Physics*, 11, 105028

- Korn, A. J., Grundahl, F., Richard, O., et al. 2007, *ApJ*, 671, 402
- Lambert, D. L. 1993, *Physica Scripta Volume T*, 47, 186
- Leenaarts, J., Rutten, R. J., Reardon, K., Carlsson, M., & Hansteen, V. 2010, *ApJ*, 709, 1362
- Lind, K., Asplund, M., & Barklem, P. S. 2009, *A&A*, 503, 541
- Mashonkina, L., Korn, A. J., & Przybilla, N. 2007, *A&A*, 461, 261
- Meléndez, J., Casagrande, L., Ramírez, I., Asplund, M., & Schuster, W. J. 2010, *A&A*, 515, L3+
- Meléndez, M., Bautista, M. A., & Badnell, N. R. 2007, *A&A*, 469, 1203
- Prantzos, N. 2012, *ArXiv e-prints*
- Ralchenko, Y., Kramida, A. E., Reader, J., & Team, N. A. S. D. 2008, *NIST Atomic Spectra Database (version 3.1.5)*
- Ramírez, I., Collet, R., Lambert, D. L., Allende Prieto, C., & Asplund, M. 2010, *ApJ*, 725, L223
- Richard, O., Michaud, G., & Richer, J. 2005, *ApJ*, 619, 538
- Samson, A. M. & Berrington, K. A. 2001, *Atomic Data and Nuclear Data Tables*, 77, 87
- Sbordone, L., Bonifacio, P., Caffau, E., et al. 2010, *A&A*, 522, A26
- Smith, V. V., Lambert, D. L., & Nissen, P. E. 1993, *ApJ*, 408, 262
- Smith, V. V., Lambert, D. L., & Nissen, P. E. 1998, *ApJ*, 506, 405
- Steffen, M., Cayrel, R., Bonifacio, P., Ludwig, H., & Caffau, E. 2010, in *IAU Symposium*, Vol. 268, *IAU Symposium*, ed. C. Charbonnel, M. Tosi, F. Primas, & C. Chiappini, 215–220